ADVANCED MATERIALS

$AgNO_3$ were 4.6 and 0.02 mol L^{-1}, respectively. The cleaned planar silicon p–n junction strips were then immediately immersed into the etching solution and treated at 50 °C for 60 min. After the etching process, the obtained samples were rinsed copiously in de-ionized water, and dried at room temperature. The thick silver film wrapping the silicon wafer was detached before examination of the sample using SEM. Samples were characterized using a SEM (JEOL JSM6301F). To prepare a TEM specimen, the sample was scraped using a knife, and the scraping was collected and suspended in ethanol; then a drop was placed on a carbon copper grid and examined in a JEOL 2010F microscope equipped with a Gatan GIF 678 system. The electronic properties of the SiNWs are characterized using CSAFM (Molecular Imaging).

Received: March 4, 2003
Final version: September 17, 2003

[1] C. M. Lieber, *Sci. Am.* **2001**, *285*, 58.
[2] Y. Cui, C. M. Lieber, *Science* **2001**, *291*, 851.
[3] Y. Cui, Q. Wei, H. Park, C. M. Lieber, *Science* **2001**, *293*, 1289.
[4] X. Duan, Y. Huang, Y. Cui, J. F. Wang, C. M. Lieber, *Nature* **2001**, *409*, 66.
[5] Y. Huang, X. Duan, Y. Cui, L. Lauhon, K. H. Kim, C. M. Lieber, *Science* **2001**, *294*, 1313.
[6] M. S. Gudiksen, L. J. Lauhon, J. Wang, D. C. Smith, C. M. Lieber, *Nature* **2002**, *415*, 617.
[7] J. T. Hu, O. Y. Min, P. D. Yang, C. M. Lieber, *Nature* **1999**, *399*, 48.
[8] M. T. Bjork, B. J. Ohlsson, T. Sass, A. I. Persson, C. Thelander, M. H. Magnusson, K. Deppert, L. R. Wallenberg, L. Samuelson, *Nano Lett.* **2002**, *2*, 87.
[9] L. J. Lauhon, M. S. Gudiksen, C. L. Wang, C. M. Lieber, *Nature* **2002**, *420*, 57.
[10] Y. Zhang, T. Ichihashi, E. Landree, F. Nihey, S. Iijima, *Science* **1999**, *285*, 1719.
[11] J. Luo, L. Zhang, Y. J. Zhang, J. Zhu, *Adv. Mater.* **2002**, *14*, 1413.
[12] W. Schwarzacher, K. Attenborough, A. Michel, G. Nabiyouni, J. P. Meier, *J. Magn. Magn. Mater.* **1997**, *165*, 23.
[13] Y. Y. Wu, R. Fan, P. D. Yang, *Nano Lett.* **2002**, *2*, 83.
[14] R. Solanki, J. Huo, J. L. Freeouf, B. Miner, *Appl. Phys. Lett.* **2002**, *81*, 3864.
[15] A. M. Morales, C. M. Lieber, *Science* **1998**, *279*, 208.
[16] J. D. Holmes, K. P. Johnston, R. C. Doty, B. A. Korgel, *Science* **2000**, *287*, 1471.
[17] W. S. Shi, H. Y. Peng, Y. E. Zheng, N. Wang, N. G. Shang, Z. W. Pan, C. S. Lee, S. T. Lee, *Adv. Mater.* **2000**, *12*, 1343.
[18] D. P. Yu, Z. G. Bai, Y. Ding, Q. L. Hang, H. Z. Zhang, J. J. Wang, Y. H. Zou, W. Qian, G. C. Xiong, H. T. Zhou, S. Q. Feng, *Appl. Phys. Lett.* **1998**, *72*, 3458.
[19] X. Y. Zhang, L. D. Zhang, G. W. Meng, G. H. Li, N. Y. Jin-Phillipp, F. Phillipp, *Adv. Mater.* **2001**, *13*, 1238.
[20] D. M. Lyons, K. M. Ryan, M. A. Morris, J. D. Holmes, *Nano Lett.* **2002**, *2*, 811.
[21] K. Q. Peng, Y. J. Yan, S. P. Gao, J. Zhu, *Adv. Mater.* **2002**, *14*, 1164.
[22] K. Q. Peng, Y. J. Yan, S. P. Gao, J. Zhu, *Adv. Funct. Mater.* **2003**, *13*, 127.
[23] S. J. Tans, A. R. M. Verschueren, C. Dekker, *Nature* **1998**, *393*, 49.
[24] T. Rueckes, K. Kim, E. Joselevich, G. Y. Tseng, C. L. Cheung, C. M. Lieber, *Science* **2000**, *289*, 94.

Electric Field Singularity Assisted Nanopatterning**

By *N. Ravishankar*,* *Vijay B. Shenoy*, and *C. Barry Carter*

Ordered arrays of metal nanoparticles on oxide substrates find diverse applications ranging from catalysis to magnetic recording, and hence patterning to produce such arrays is an area of considerable technical importance and active research.[1–6] A majority of ongoing approaches relies on the use of pattern-transfer onto suitable substrates followed by a deposition procedure. Patterning based on self-assembly,[2] lithography techniques,[7] focused ion beam (FIB) lithography,[8] electrodeposition,[9] and soft lithography[6] are commonly used. Ordered nanoparticles of semiconductors,[10] magnetic materials,[5,9,11–13] transition metal catalysts,[1,3] microelectronic materials,[14,15] and optical/optoelectronic materials[16] have been produced using these techniques or variations thereof. The drawbacks of the popular photolithography technique arise due to the limitations imposed by optical diffraction, which implies that only features with lateral dimensions larger than 100 nm can be produced.[6] Newer techniques using electron beams[1] or FIBs[8,17] have been used to produce features as small as a few nanometers. The advent of newer non-photolithographic techniques like soft lithography provide techniques to produce feature sizes ranging from 30 nm to 100 μm.[6] Electrodeposition has also been used to produce ordered arrays/nanowires on stepped surfaces.[18,19]

In this report, we introduce a new non-lithographic method for producing ordered arrays of metal particles on a reconstructed ceramic surface. This method takes advantage of the stepped structure that is formed as a result of annealing a high-energy alumina surface that serves as a template for producing arrays of metal nanoparticles. Although the principle of using surface steps as decoration sites has been used extensively, patterning of metal particles that is shown here has a different physical origin to these well-known step decoration techniques.[20] In these decoration techniques, nucleation takes place under conditions of supersaturation at the lower

[*] Dr. N. Ravishankar, Dr. V. B. Shenoy
Materials Research Centre
Indian Institute of Science
Bangalore 560 012 (India)
E-mail: nravi@mrc.iisc.ernet.in
Prof. C. B. Carter
Dept. of Chemical Engineering and Materials Science
University of Minnesota
421 Washington Ave. S.E., Minneapolis, MN 55455 (USA)

[**] The authors acknowledge Prof. Ashutosh Sharma, Prof. K. Chattopadhyay, Prof. Vikram Jayaram, and Shelley Gilliss for useful discussions. VBS acknowledges support from DST, Government of India under Fast Track Scheme. CBC acknowledges the U.S. Department of Energy (Grants DE-FG02–92ER45465-A004 and DE-FG02–01ER45883) for financial support.

 © 2004 WILEY-VCH Verlag GmbH & Co. KGaA, Weinheim DOI: 10.1002/adma.200305337

sides of the steps (equivalent to the valley sites in our case). Further, nucleation also occurs on impurities and defects on the flat terrace regions. The spacing of the clusters in these decoration experiments is governed by the diffusion of atoms along the steps and is shown to be inversely proportional to the square root of the width of the step.[21] In the present work, however, we show that nucleation occurs under conditions of undersaturation at the top side of the step (crests). Nucleation in the present case is highly site-specific to the crests owing to strong electrostatic effects. Additionally, the particle spacing increases with the width of the step. The $(10\bar{1}0)$ surface, the *m*-plane of alumina, is an unstable plane and reconstructs into a hill-and-valley structure on annealing at high temperatures. Figure 1 is a secondary-electron (SE) image of such a surface. The $\{\bar{1}012\}$ and $\{10\bar{1}\bar{1}\}$ facets that are formed as a result of this reconstruction have different surface

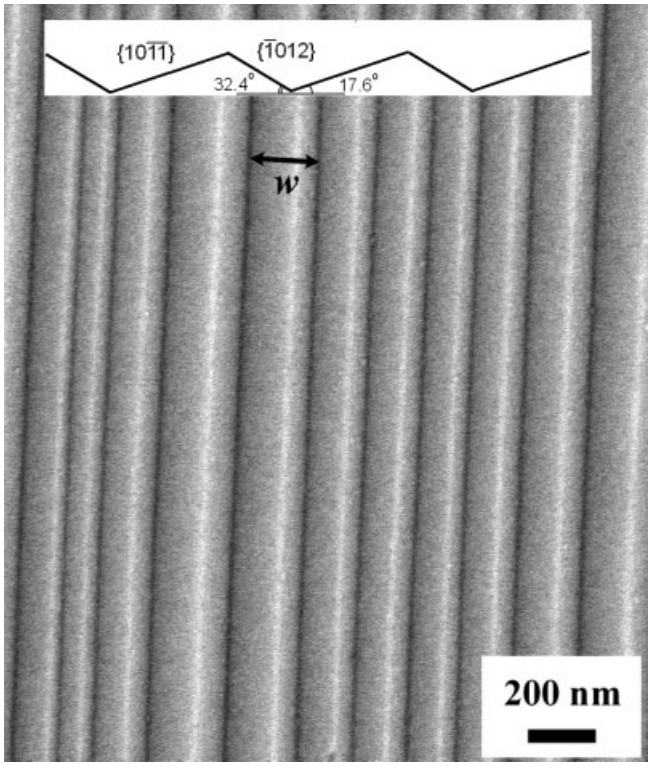

Figure 1. SE image of a reconstructed alumina surface showing the hill-and-valley structure that is formed. The surface was annealed in air at 1400 °C for 16 h. The inset at the top (not to scale) schematically illustrates the indices of the facets that are formed as a result of the annealing and the angular relationship between the facets.

energies and make angles of 32.4° and 17.6°, respectively, (see inset, Fig. 1) with the original *m*-plane.[22,23] Atomic force microscopy (AFM) analysis reveals that the height and the spacing between steps are ~25 nm and ~150 nm, respectively. The reconstruction is not restricted to local regions and is seen throughout the sample (~2 mm × 2 mm).

A schematic of the experimental conditions that were used to produce the ordered arrays is shown in Figure 2. Under the

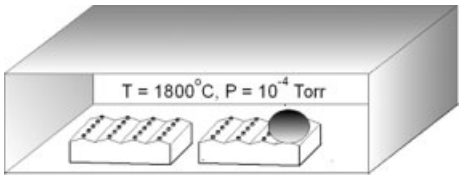

Figure 2. A schematic of the vacuum chamber used for producing the nanoarrays. A small foil of Pt is placed on a reconstructed alumina surface (2 mm × 2 mm) and heated to 1800 °C under a vacuum of 10^{-4} torr. Pt transport to the crests of the reconstructed structure takes place via vapor-phase transport corroborated by the formation of nanoparticles on a second alumina surface placed adjacent but not in contact with the first one.

experimental conditions, as shown schematically, a droplet of liquid Pt forms on the surface. An SE image from a region adjacent to the large Pt droplet (Fig. 3A) shows Pt particles having a size range of 30–50 nm with a spacing of 50–120 nm, perched on the crests of the reconstructed surface. The size of the particles and their spacing is very uniform along any particular ridge. The size of the particles, although uniform on a given ridge, increases as the width, *w*, of the ridge increases. Larger particles are more widely spaced and in some cases have smaller particles in between (as shown in the inset). The

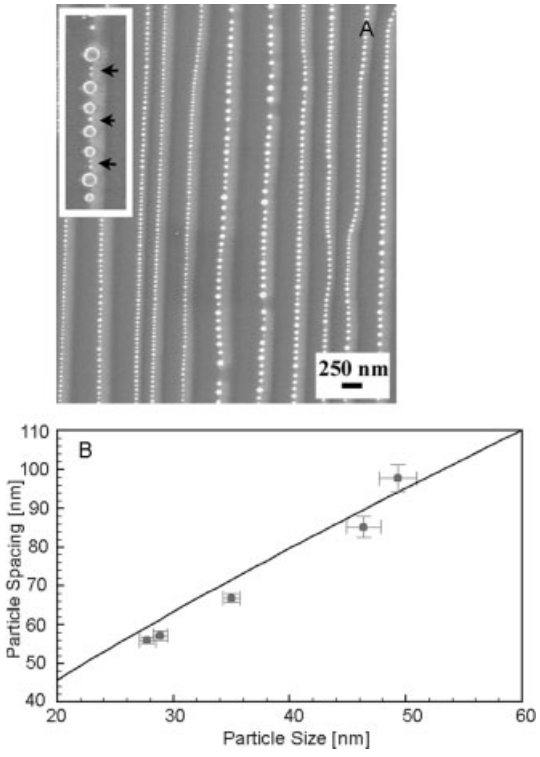

Figure 3. A) Arrays of Pt nanoparticles on a reconstructed alumina surface. The particles form by a vapor-phase transport mechanism. The size of the particle array on a particular ridge depends on the width of the ridge. A magnified inset shows the presence of smaller particles in between large particles. B) Variation in the spacing of the particles as a function of the particle size. The solid line corresponds to a fit of the experimental data to the theoretical relation $l \sim s^{0.8}$ where *l* and *s* are, respectively, the particle spacing and size.

 © 2004 WILEY-VCH Verlag GmbH & Co. KGaA, Weinheim

ADVANCED MATERIALS

dependence of the spacing of the particles on their size is shown in Figure 3B indicating that the spacing increases with increasing particle size. There is considerable coarsening of the step structure and disordering of the steps as a result of the high-temperature heat treatment under vacuum conditions and hence some of the steps appear curved in the images shown in Figure 3A. Nanoparticles also form on an alumina surface that was placed adjacent to, but not in contact with the surface that contained the Pt foil (see Fig. 2).

The following questions arise from the observations mentioned above. How do the Pt nanoparticles form and why are they so uniform in size along a given ridge? Why do these particles populate only the crest regions on the reconstructed surface? And, why does the spacing between the particles depend on their size? These can be answered by considering the following steps in the formation of the nanoparticle arrays. The process of formation of the ordered array of particles consists of three steps:

1. Liquid Pt from the large droplet goes to vapor phase under conditions of high vacuum and temperature.

2. Although the vapor pressure of Pt corresponds to undersaturation, it condenses on the crests on the alumina surface, aided by the electric-field singularities at the crests. The equilibrium configuration of the condensed liquid is a string of equally sized/spaced droplets perched on the crests, resulting from a competition between the surface and electrostatic energies.

3. These droplets freeze on cooling to give rise to the ordered array of nanoparticles.

The equilibrium vapor pressure of Pt at the melting point (1769 °C) is 2×10^{-4} torr.[24] Although the complete equation of state for Pt is unknown, it is clear that the temperature (T) and pressure (P) that is maintained in the present experiment is in the vapor-phase regime in the P–T phase diagram of Pt. Under these conditions, there is a driving force for the Pt liquid to go into the vapor phase while the nucleation of liquid from the vapor phase is energetically unfavorable. On evaporation, Pt atoms are transported away from the molten Pt surface by vapor-phase diffusion. The role of vapor-phase transport on the formation of Pt particles in the present case is corroborated by the presence of Pt nanoparticles on an alumina surface that was placed adjacent to, but not in contact with the sample that contains the large Pt droplet. To further corroborate this point, two sets of experiments were performed separately with Au and solder (Pb–Sn alloy) liquids with temperatures close to their melting points (1200 °C for Au and 400 °C for Pb–Sn alloy). Here, no particles were seen in the region adjacent to the large droplet. The equilibrium vapor pressure of these materials (10^{-5} torr for Au and $\sim 10^{-10}$ torr for a Pb–Sn alloy)[24] is much lower than the operating pressure (10^{-4} torr) in the experiment and thus there is no driving force for the atoms to go to the vapor phase, and hence no possibility of condensation and formation of nanoparticles.

Nucleation of a liquid from a vapor phase, as analyzed by the classical nucleation theory, involves an increase in energy due to the formation of a surface (surface energy γ) that is offset by the decrease in volume free energy (ΔG_v) for the transformation. This competition leads to an activation barrier and a critical size, r^*, above which a nucleus becomes stable.[25,26] The vapor phase that forms in the case of Pt is undersaturated ($\Delta G_v \geq 0$), i.e., there is no possibility of homogeneous nucleation of the liquid phase under such conditions.

The role of foreign surfaces in promoting nucleation by reducing the activation barrier is a well recognized, widely used fact.[25–29] Heterogeneous nucleation from the vapor phase has been shown to be a powerful technique to detect extremely small levels of impurities on surfaces.[30] For the nucleation of liquid from a supersaturated vapor, the reduction in the activation barrier depends upon the geometry of the surface and the contact angle of the liquid on this surface. Although the activation barrier is reduced for heterogeneous nucleation for the geometry of the reconstructed surface, there is still a need for a finite supersaturation for the formation of the liquid phase.[26] Decoration of surface ridges by heterogeneous nucleation on wedged surfaces with different contact angles and wedge angles has been investigated in detail.[31] It has been shown that for values of enclosed angle of the wedge, which are less than 180°, the crests are never decorated. Formation of nuclei on a flat surface, or even in the valleys between the crests, is more favorable. Thus, in the present case, the questions remain as to why the liquid condenses at all, and, why does it decorate the crests and not the valleys?

The answer lies in the fact that nucleation of Pt takes place on the surface of an ionic material. The role of electrostatic fields in promoting nucleation is well documented, and, for example, is the basis for the Wilson cloud chamber.[26,32] The surface of alumina, an ionic material, which possesses an excess electrostatic potential, V,[33] serves to promote the nucleation process. The excess electrostatic potential, V, is due the equilibration of ionic defects with the free surface of the material[33] and is insensitive to the details of ionic arrangement on the surface. Due to the hill-and-valley geometry of the alumina surface, the resulting electric field near the surface is highly inhomogeneous. In particular, the electric field near the tip of the crest,[34] with enclosed angle α (= 130°, Fig. 4) varies as $\rho^{-\beta}$, where ρ is the distance from the tip and $\beta = (\pi - \alpha)/(2\pi - \alpha) = 0.22$. We note here that this form of an electric field singularity can be generated near any surface (even in a non-ionic material) maintained at a constant electric potential and having a corrugated structure.

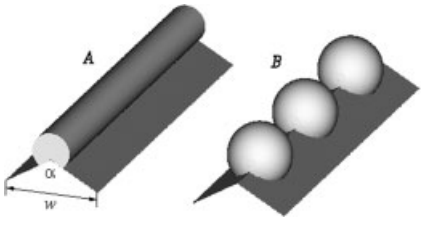

Figure 4. Schematic illustration of the formation of a continuous tube on the crest (A) and an array of equally sized and spaced droplets (B). Configuration B is the thermodynamically favored state for the Pt droplets on the alumina surface owing to a competition between capillary and electrostatic forces.

 © 2004 WILEY-VCH Verlag GmbH & Co. KGaA, Weinheim

The formation of a metal droplet covering the crest reduces the electrostatic energy of the system. In the present case ($\beta = 0.22$), assuming that the liquid condenses in the form of a tube covering the crest (indicated as configuration A in Fig. 4), the free energy change per unit length for the formation of a tube of radius r is $A\gamma r - Cr^{2(1-\beta)}$, where A is a non-dimensional constant of order unity, and C is a positive constant that depends on the electrostatic parameters. The volume-free-energy term has been neglected since the experiments are carried out very close to the liquid–vapor coexistence line in the P–T diagram (i.e., $\Delta G_v \sim 0$). The free energy expression contains two terms, the surface energy term that increases the free energy and dominates at small values of r, and the electrostatic term that reduces the free energy of the system and dominates at larger values of r. The electrostatic term plays a role similar to that of the volume term (during homogeneous nucleation) in reducing the free energy and aids heterogeneous nucleation from the undersaturated vapor phase. Thus, nucleation of liquid metal on the crests is aided by the presence of a singularity in the electric field ($\rho^{-0.22}$). Further, there is no singularity near the corner of the valleys (electric field scales as $\rho^{0.38}$). In fact, the magnitude of the electric field increases away from the corners of the valleys and the liquid metal is repelled from the valley corners. Therefore, the crests of the surface are the most favored sites for nucleation owing to the presence of a singularity in the electric field.

The thermodynamically favored configuration of the liquid that condenses on the crests is not a tube of liquid (configuration A in Fig. 4), as considered above for the sake of illustration, but a string of equally sized and regularly spaced droplets (configuration B in Fig. 4). This is due to a competition between the surface energy, which favors formation of droplets (similar to Rayleigh–Plateau instability),[35] and the electrostatic energy, which favors a continuous liquid tube so that most of the crest is covered with liquid metal. This competition is governed by the relative magnitudes of two length scales present in the system. The first is a length scale associated with the ratio of the surface and electrostatic energies given as $\lambda_0 = (\gamma/C)^{1/(1-2\beta)}$. The second scale is set by $\sqrt{v_0}$, where v_0 is the average volume of liquid metal that has condensed per unit length of the crest. The spacing of the particles can be obtained by considering a metastable configuration of the liquid metal in the form of a continuous tube (configuration A in Fig. 4) of radius $r_0 \sim \sqrt{v_0}$. The geometry of the tube is perturbed by a sinusoidal variation of its radius as $r(z) = r_0(1 + S\cos(\boldsymbol{k}z))$, ($S$ is a non-dimensional amplitude of the perturbation, $\boldsymbol{k}$ is the wavevector of the perturbation, and z is the distance along the cylinder axis) and the change in the free energy is evaluated. The analysis indicates that perturbations with wavevectors smaller than a critical wavevector $\boldsymbol{k}_c$ reduce the free energy of the system implying that the equilibrium configuration of the condensed liquid is a set of equally spaced droplets as shown in configuration B of Figure 4. The spacing l ($\sim 1/\boldsymbol{k}_c$) of the droplets is determined as $l/\lambda_0 \sim (v_0/\lambda_0^2)^{(1+2\beta)/4}$. The size of the particles, s, obtained using volume conservation ($s^3 \sim v_0 l$) *is* $s \sim (v_0)^{(5+2\beta)/12}$ resulting in the relationship between spacing and size as $l \sim s^{(3(1+2\beta))/(5+2\beta)}$. Substituting $\beta = 0.22$, the spacing of the particles is related to the size as $l \sim s^{0.8}$. A fit of this relation with experimental data shows excellent agreement (see Fig. 3B).

The quantity v_0, the volume of the liquid condensed per unit length of the ridge, is directly proportional to the width, w, of the ridge (see Fig. 4). Therefore, particles on wider ridges (larger w) are larger as is evident from Figure 3A. Also, since wider ridges have particles spaced further apart, the regions of the crest between the particles exposed to vacuum are locations of very high electric field. Thus, fresh nucleation can occur between the large particles and the configuration in this case can be an array of very large particles with intermediate particles in between, as is seen in the inset in Figure 3A.

The regular arrangement of nanoparticles of platinum on the crests of the alumina surface is a frozen equilibrium configuration of liquid platinum that condenses in the form of an array of regular droplets. We estimate the time Δt required for collecting an amount of liquid platinum such that the volume per unit length on the crest is v_0 to be

$$\Delta t = 2\sqrt{mkT}\, v_0/(pw\Omega) \quad (1)$$

where p is the pressure, m is the mass of a Pt atom, k is the Boltzmann constant, T is the temperature, and Ω is the volume per atom. For $v_0 = 100$ nm^2, this time interval is estimated to be about 4 s. Equilibration time scales for the liquid at these temperatures can hardly be larger than 10^{-6} s owing to very high mobility of atoms (large surface diffusion) and a relatively low viscosity of liquid metals ($< 5 \times 10^{-3}$ N s m^{-2}). The time required for equilibration is much smaller than the time required for mass transport from the vapor phase to the droplet and thus the droplet array is always in equilibrium.

We have established a novel method for the preparation of regular arrays of metal nanoparticles. The main idea is to exploit the reconstructed surfaces of ionic solids, which have a hill-and-valley structure and thus singularities in the electric fields that exist along the surface. This enables the preferential condensation of liquid metal on the crests in the form of an array of droplets. The size and spacing distribution is controlled by the geometry of the surface. By a suitable choice of annealing temperature and time, it is possible to vary the length scale of reconstruction of the surface and thus control the size and spacing of the droplets that form on this surface.

For any given metal/alloy, it is possible to choose the temperature and pressure ranges and surfaces with different potency for heterogeneous nucleation, such that ordered arrays of nanoparticles can be produced using this method. Although the method has been demonstrated for the case of nucleation from the vapor phase, it is possible to envisage extensions of this method to produce arrays of nanoparticles by precipitating from a solution on suitably ridged surfaces with electric field singularities. The method therefore holds promise of application to a wide class of material systems.

 © 2004 WILEY-VCH Verlag GmbH & Co. KGaA, Weinheim

ADVANCED MATERIALS

The use of electrostatic forces to align nanoparticles, termed nanoxerography, has been demonstrated earlier.[36] However, this method is primarily an alignment method and requires nanoparticles produced elsewhere. The present work relies on an in-situ nucleation and ordering of nanoparticles and the resolution obtained here is much better than in the reported nanoxerographic techniques. An additional advantage of the present technique is that the nanoparticles that form on solidification have a crystallographic alignment on the surface as is evident from the alignment of the faceted particles in the SE image shown in Figure 5. This has very important implications for the properties of such arrays. For instance, aligned

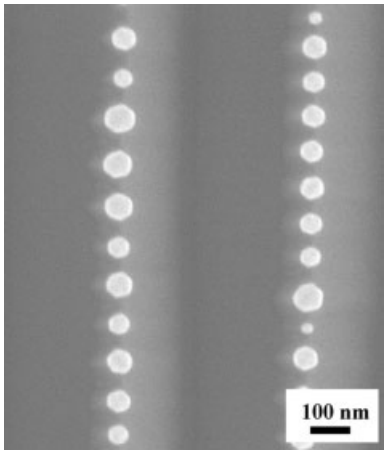

Figure 5. High-magnification image of the Pt nanoparticles on the alumina surface showing the faceted nature of the particles. The alignment of the facets indicates a crystallographic orientation for the particles.

ferromagnetic nanoparticles have a tremendous potential for recording applications. Of course, the magnetic anisotropy of the particles becomes important in this case. It is interesting to note that arrays of ferromagnetic particles of comparable dimensions and spacing on the *m*-plane translates to an areal density of 10^{11} per square inch (1 $in^2 = 6.45\,cm^2$).

Experimental

Substrate Preparation: Single crystals of Al_2O_3, 1 mm thick and polished both sides (Crystal Systems, MA) were used as substrates. The substrates were annealed at 1400 °C for 16 h in air in a box furnace in flat alumina boats covered with an inverted alumina crucible. High-purity alumina powder was packed in the boat in the region outside the crucible and acts as a getter for impurities. The substrates were cleaned ultrasonically in acetone, followed by methanol prior to the annealing treatment.

Formation of Pt Nanoarrays: For the vapor-phase transport of Pt on to the reconstructed substrates, a thin foil of high-purity Pt (approximately 0.5 mm × 0.5 mm × 0.01 mm thick) served as the source of metal. The foil was placed on the reconstructed surface and the assembly was heated to 1800 °C in a vacuum furnace (Centorr, NH) under a vacuum of $\approx 10^{-4}$ torr and a molten droplet of Pt (larger than 100 μm in diameter) forms on the surface at this temperature. A nominal heating rate of 20 °C min^{-1} was used. The power to the furnace was switched off after holding the assembly at this temperature for a very short time (< 2 min). The exact cooling rate was not calculated but the initial cooling rate was estimated to be ≈ 100 °C min^{-1}.

SEM Observation: A field-emission SEM (Hitachi S900) operated at 5 kV was used. Imaging was done in the SE imaging mode. A thin layer of Pt (1–2 nm) was used to prevent charging in the microscope.

Received: May 2, 2003
Final version: September 26, 2003

[1] J. Zhu, G. A. Somorjai, *Nano Lett.* **2001**, *1*, 8.
[2] D. M. Dabbs, I. A. Aksay, *Annu. Rev. Mater. Sci.* **2000**, *51*, 601.
[3] H.-J. Freund, *Surf. Sci.* **2002**, *500*, 271.
[4] D. Martrou, P. Gentile, N. Magnea, *J. Cryst. Growth* **1999**, *201*, 101.
[5] J. Shen, J. Kirschner, *Surf. Sci.* **2002**, *500*, 300.
[6] Y. Xia, G. M. Whitesides, *Annu. Rev. Mater. Sci.* **1998**, *28*, 153.
[7] R. F. W. Pease, *J. Vac. Sci. Technol. B* **1992**, *10*, 278.
[8] S. Matsui, Y. Kojima, Y. Ochiai, *Appl. Phys. Lett.* **1988**, *53*, 868.
[9] S. Ming, G. Zangari, M. Shamsuzzoha, R. M. Metzger, *Appl. Phys. Lett.* **2001**, *78*, 2964.
[10] J. L. Coffer, S. R. Bigham, L. Xin, R. F. Pinizzotto, R. Young Gyu, R. M. Pirtle, I. L. Pirtle, *Appl. Phys. Lett.* **1996**, *69*, 3851.
[11] Z. Ziyi, B. Gates, X. Younan, Q. Dong, *Langmuir* **2000**, *16*, 10 369.
[12] W. Weijia, W. Ning, D. W. Zhang, C. Chen, K. N. Tu, *J. Mater. Res.* **1999**, *14*, 1186.
[13] M. R. Scheinfein, K. E. Schmidt, K. R. Heim, G. G. Hembree, *J. Appl. Phys.* **1996**, *79*.
[14] Q. T. Zhao, L. Kappius, S. Mesters, S. Mantl, *Proc. SPIE-Int. Soc. Opt. Eng.* **1999**, *3881*, 77.
[15] H. Morimoto, Y. Sasaki, H. Onoda, K. Tsukamoto, T. Kato, *Jeol News* **1986**, 49.
[16] W. Gotschy, K. Vonmetz, A. Leitner, F. R. Aussenegg, *Appl. Phys. B* **1996**, *63*, 381.
[17] S. Matsui, Y. Kojima, Y. Ochiai, T. Honda, *J. Vac. Sci. Technol. B* **1991**, *9*, 2622.
[18] S. Morin, A. Lachenwitzer, O. M. Magnussen, R. J. Behm, *Phys. Rev. Lett.* **1999**, *83*, 5066.
[19] M. P. Zach, K. H. Ng, R. M. Penner, *Science* **2000**, *290*, 2120.
[20] M. Krohn, *Vacuum* **1987**, *37*, 67.
[21] A. D. Gates, J. L. Robins, *Surf. Sci.* **1982**, *116*, 188.
[22] J. R. Heffelfinger, C. B. Carter, *Surf. Sci.* **1997**, *39*, 188.
[23] J. R. Heffelfinger, M. W. Bench, C. B. Carter, *Surf. Sci.* **1995**, *343*, L1161.
[24] J. F. van der Veen, B. Pluis, A. W. Denier van der Gon, in *Chemistry and Physics of Solid Surfaces VII* (Eds: R. Vanselow, R. Howe), Springer Verlag, Berlin **1988**, p. 455.
[25] J. W. Christian, in *The Theory of Transformations in Metals and Alloys*, Pergamon Press, Oxford **1981**, p. 180.
[26] J. P. Hirth, G. M. Pound, *Progress in Materials Science* (Ed: B. Chalmers), Vol. 11, Pergamon Press, Oxford **1963**, p. 190.
[27] L. Mederos, A. Quintana, G. Navascues, *J. Chem. Phys.* **1984**, *81*, 4630.
[28] K. Padilla, V. Talanquer, *J. Chem. Phys.* **2001**, *114*, 1319.
[29] D. Turnbull, *J. Chem. Phys.* **1950**, *18*, 198.
[30] T. D. Lee, F. Spaepen, J. A. Golovchenko, *MRS Proc.* **1997**, *477*, 409.
[31] C. A. Sholl, N. H. Fletcher, *Acta Metall.* **1970**, *18*, 1083.
[32] P. Grinfeld, *Phys. Rev. Lett.* **2001**, *87*, 095701/1.
[33] W. D. Kingery, H. K. Bowen, D. R. Uhlmann, *Introduction to Ceramics*, John Wiley and Sons, New York **1975**.
[34] J. D. Jackson, *Classical Electrodynamics*, John Wiley and Sons, New York **1999**.
[35] L. Rayleigh, *Philos. Mag.* **1892**, *34*, 144.
[36] H. O. Jacobs, S. A. Campbell, M. G. Steward, *Adv. Mater.* **2002**, *14*, 1553.

 © 2004 WILEY-VCH Verlag GmbH & Co. KGaA, Weinheim